ELSEVIER

Contents lists available at ScienceDirect

Computers in Biology and Medicine

journal homepage: www.elsevier.com/locate/compbiomed



A comprehensive physics-based model for the brachial Artery's full flow mediated dilation (FMD) response observed during the FMD test

Bchara Sidnawi ^{a,b}, Bingjie Zhou ^{a,b}, Zhen Chen ^c, Chandra Sehgal ^c, Sridhar Santhanam ^a, Qianhong Wu ^{a,b,*}

- ^a Department of Mechanical Engineering, Villanova University, PA, 19085, USA
- ^b Cellular Biomechanics and Sport Science Laboratory, Villanova University, PA, 19085, USA
- ^c Department of Radiology, University of Pennsylvania, PA, 19104, USA

ARTICLE INFO

Keywords: Flow mediated dilation Brachial FMD test Fluid-structure interaction Mechanotransduction Wall shear stress Model

ABSTRACT

In this study, a physics-based model is developed to describe the entire flow mediated dilation (FMD) response. A parameter quantifying the arterial wall's tendency to recover arises from the model, thereby providing a more elaborate description of the artery's physical state, in concert with other parameters characterizing mechanotransduction and structural aspects of the arterial wall. The arterial diameter's behavior throughout the full response is successfully reproduced by the model. Experimental FMD response data were obtained from healthy volunteers. The model's parameters are then adjusted to yield the closest match to the observed experimental response, hence delivering the parameter values pertaining to each subject. This study establishes a foundation based on which future potential clinical applications can be introduced, where endothelial function and general cardiovascular health are inexpensively and noninvasively quantified.

1. Introduction

Brachial artery flow mediated dilation (FMD) is a widely reported clinical practice, based on which the integrity of arterial walls, a key indicator of cardiovascular health, is assessed. After having a pressure cuff wrapped around a subject's upper arm while lying supine (Fig. 1a), the cuff is inflated to a certain pressure, long enough to cut off the blood flow to the lower arm, thereby collapsing the brachial artery. The cuff is then abruptly deflated, and the arterial diameter (Fig. 1c) response is monitored via ultrasound imaging (Fig. 1b), until full recovery. Fig. 1c shows the phases of a typical FMD response where the diameter initially rises before it briefly dwells around a peak value, generally exceeding its baseline as measured before the test, which is then followed by a recovery phase where the arterial diameter eventually returns to said baseline. Fig. 1d shows a diagram illustrating the interplay between arterial wall shear stress (WSS), arterial compliance, and arterial diameter underlying the FMD response, which is enabled by the diffusion of vasodilators, represented here by a dilation stimulation signal, s, which will be discussed in detail later in the Formulation section. The blue curves represent the distribution of s in the radial direction, r, at different instants (hence the t arrow indicating their chronological order). This concept was introduced in our earlier study on the subject [1]. A WSS spike is picked up by the arterial wall through mechanotransduction, which is how flow conditions are communicated to the endothelial cells (ECs) lining the inner walls of blood vessels, initiating the diffusion of a vasodilation signal that prompts the wall's outer layers to change their compliance. Under the blood pressure, pushing outward, the arterial diameter changes accordingly, altering flow conditions, hence affecting the WSS that started the entire process, completing the feedback loop.

Comparing the peak diameter to its baseline value throughout the response provides a commonly used dilation metric, FMD%, that can serve as a quantitative description for the physical state of the arterial wall. The appealing aspects of the FMD test are its affordability and safety. Abnormal FMD% levels have been linked to smoking, renal dysfunction, and visceral obesity [2–5]. Brachial Artery Flow-Mediated Dilation's (BAFMD) utility for assessing cardiovascular health and diagnosing cardiovascular diseases based on FMD% has been further established by other studies [6–9]. Moreover, according to a recent comprehensive review [10] dedicated to how the virus affects the heart and blood vessels, SARS-CoV-2 has been associated with leaky vessels, pointing to a compromised glycocalyx layer and endothelial function,

^{*} Corresponding author. Department of Mechanical Engineering Villanova University, 800 Lancaster Ave, PA, 19085, USA. *E-mail address:* qianhong.wu@villanova.edu (Q. Wu).

which therefore suggests that such changes could be picked up by this test. However, solely relying on the artery's peak percent dilation (FMD %) as a descriptor of arterial health overlooks crucial information that parts of the response, other than the peak, have to offer [11]. This paper aims to provide a theoretical framework through which any observed FMD response can be scrutinized in much greater detail for a more nuanced arterial health assessment.

Mechanotransduction, the sensing and transmission of mechanical stimuli, is what lies at the heart of FMD. The endothelial glycocalyx layer (EGL), a porous microstructure of proteoglycans and glycoproteins extending from the endothelial cells (ECs) lining blood vessels' inner surface [12,13], picks up mechanical signals carrying information about the flow environment, and relays them to the ECs surface. The ECs then initiate biochemical signal pathways through which the outer layers of

the arterial wall are instructed to constrict or dilate accordingly to accommodate changes in flow conditions. This role of the EGL is well established [12,14–18]. Extensive experimental, analytical, and numerical studies have been conducted to probe mechanotransduction on the cellular level [19–29]. The most crucial findings of those studies established the necessity of the EGL and ECs for a functioning mechanotransduction [24–26], and the dependence of Nitric Oxide (NO, a prominent vasodilator) production by the ECs, on WSS level sensed at the EGL [21,28,29]. The EGL and ECs have been shown to exhibit a bias towards non-oscillatory, undisturbed WSS patterns. Only an added forward component to a disturbed or oscillatory WSS signal could trigger the EGL's structural remodeling in-vitro [30]. In another study, prolonged exposure of ECs to a laminar flow significantly boosted their WSS-induced release of vasodilators [31]. NO synthesis has been shown

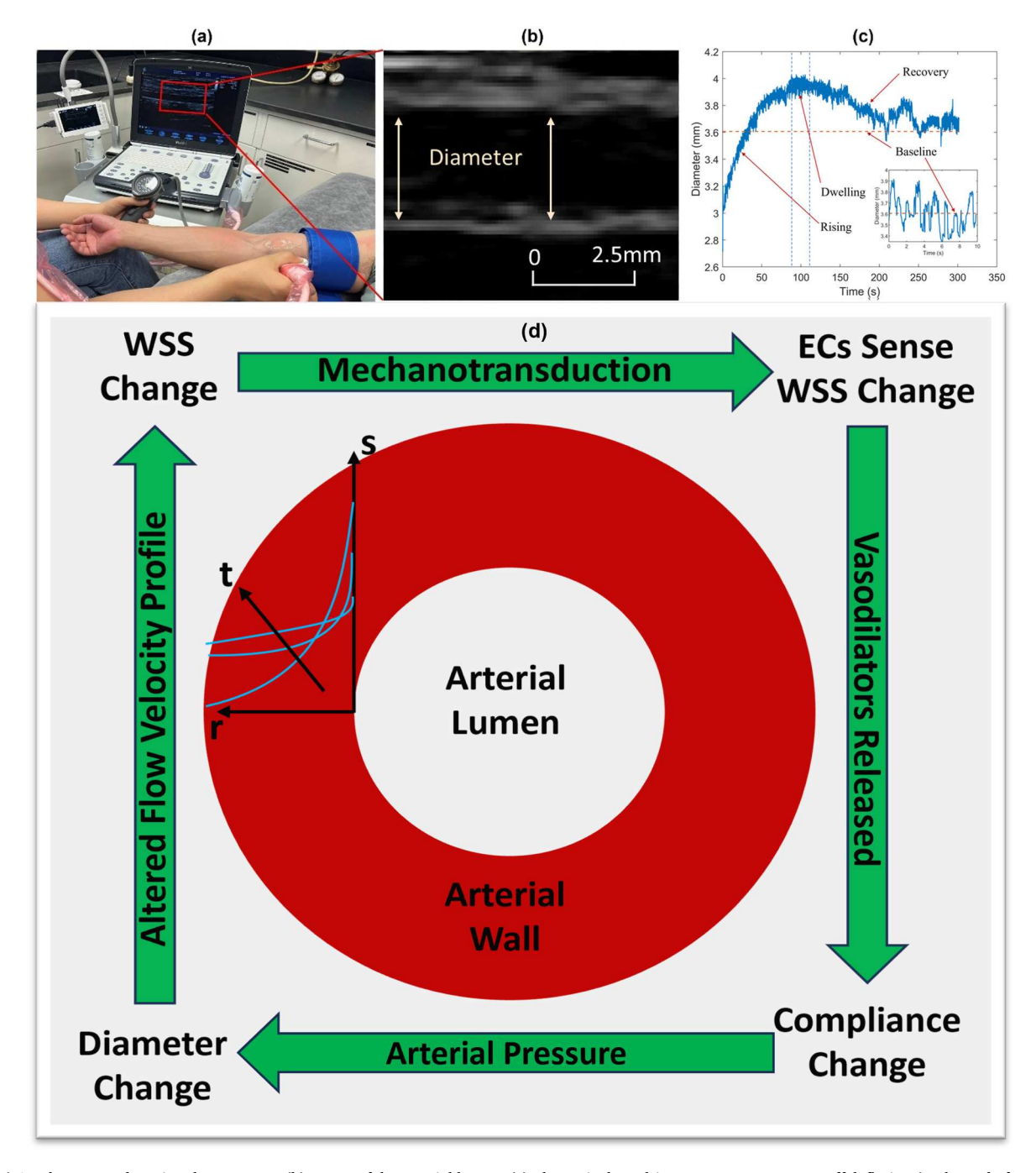


Fig. 1. (a) A volunteer undergoing the FMD test. (b) Image of the arterial lumen. (c) The typical resulting FMD response post cuff deflation (at the end of a 5-min-long inflation). x-axis: time (seconds) y-axis: Arterial diameter (mm). (d) An illustration of the mechanism underlying the arterial FMD response shown in (c).

to be dependent on the step-change magnitude of WSS, while a turbulent flow failed to prompt NO production [32]. Driven by this cohort of studies on the connection between WSS and vasodilation stimulation, our group hypothesized a mechanism (Fig. 1d) by which mechanotransduction is manifested in the FMD response and formulated a mathematical model that successfully reproduced its rising-and-dwelling part [1,33].

Our first study [33] has the limitation of assuming that the arterial wall is a thin elastic cylindrical shell, which misses the signal diffusion aspect of the real process. However, the model based on that assumption still managed to predict the gradual steepening (rather than abrupt springing) arterial expansion observed in the early part of the FMD response, as a hallmark of mechanotransduction, as shown in Fig. 1c. The thin wall assumption was later addressed in our second study [1], where the vasodilation signal diffusion through the wall's thickness is accounted for. The improved model not only reproduced the hallmark of mechanotransduction in the observed FMD response, but also predicted the arterial outer-to-inner diameter ratio within a reasonable margin. Three physically sensible parameters emerged from that model, as additional measures of arterial health. These are the Arterial Sensitivity to WSS, the Minimum Arterial Stiffness Ratio, and the Arterial Mechanotransduction Strength. The premise shared by the first two studies is that the arterial wall's response is primarily elastic. This was confirmed in our third study on the subject [34], where the significance of a viscous contribution to the FMD response is found to be negligible. The missing piece that all three studies never touched on though, is the response's recovery phase, in which the diameter recedes to its baseline value as shown in Fig. 1c.

This paper seeks to fill this gap, as well as addressing a common limitation of other studies in the literature that did reproduce the FMD response through mathematical modeling. In particular, a study by Yamazaki and Kamiyama [35,36] analyzed the biochemical pathways involved in the process with impressive rigor and successfully replicated a typical FMD response. However, their approach's heavy reliance on biochemical analysis limits its applicability to FMD responses that result from the lower-arm cuffing protocol that they followed. This is because the role of NO in vasodilation is diminished when upper-arm cuffing is used, where other compounds such as Endothelium-Derived Hyperpolarizing Factor (EDHF) also play important roles [37], and where the observed FMD% is generally higher. The authors also seem to treat the artery as thin walled, where the stress is uniform across the thickness. In another, more recent study [38], NO diffusion throughout the wall was incorporated in analyzing the brachial artery's behavior during the recovery phase of a lower-arm-cuffing FMD test. Rather than allowing for variability between individuals though, the model's parameters characterizing the interaction among WSS, NO production, and arterial stiffness, were obtained from in-vitro, rather than in-vivo experiments. Also, an overall wall stiffness was used, and related to a thickness-averaged vasodilator concentration, while our previous two studies [1,34] (as well as the current one) account for the local vasodilator effect on the space-and-time-dependent stiffness, albeit through a conceptual property as a surrogate to the vasodilator concentration (See Fig. 1d).

In the current study, for the first time, a complete phenomenological model, rooted in first principles, is developed to describe an entire FMD response, irrespective of the cuffing protocol. The parameters arising from the model, and which collectively serve as a quantitative description of the arterial state, were adjusted to produce a response that matched its experimental counterpart extracted from healthy volunteers. The new parameter among those is one that characterizes the arterial wall's drive for recovery, thereby providing a more complete description of the artery's physical state.

The remainder of this paper is structured as follows: (1) A *Methods* section where the performed experimental work, along with the mathematical development of the proposed model are described; (2) a *Results and Discussion* section, where matching the theoretical FMD response to

its experimentally observed counterpart is presented; (3) a section where further elaboration on the effect of the recovery parameter is provided; (4) a section where the matching algorithm that we used is outlined; and (5) a *Conclusion* section where the study's findings and limitations are summarized, and future directions are proposed.

2. Methods

2.1. Experiment

The experimental protocol was approved by the institutional review committee and informed consent for the study was obtained from all human subjects in accordance with the World Medical Association Declaration of Helsinki: Ethical principles for medical research involving human subjects, 2008. The study's approval number and date are IRB-FY2023-127, and 05/05/2023, respectively. Healthy volunteers underwent FMD tests (Fig. 1a-c) in the Cellular Biomechanics and Sports Science Lab at Villanova University (Vivid I ultrasound machine, 10 MHz linear array, GE Healthcare, Carmel, ISRAEL). After 5 min of blood flow obstruction by means of an inflated pressure cuff (~50 mmHg above systolic pressure) wrapped around the subject's upper arm (Fig. 1a), the cuff is deflated, and the artery is monitored with an ultrasound scanner for the next 5 min (Fig. 1b). Twelve datasets, from 4 female and 8 males (6 Asian and 6 White. Age range: 20 – 75 years, Mean age: 35.3 years, SD: 16.31 years) that are minimally noisy over the entire post-deflation monitoring period were obtained by postprocessing the recorded clips in MATLAB (Fig. 1c). As may be gleaned from one of our previous studies [1], it is easier to achieve low-noise readings when only the rising-and-dwelling part is considered. However, towards the recovery phase of the response, the subjects become more likely to experience some restlessness, and hence involuntary movements can occur. The sonographer may also feel a little sore trying to maintain a fixed posture to hold the probe at a particular angle for 5 min straight, making a few reflexive adjustments inevitable, thereby affecting the images' quality. Nevertheless, as this study is about illustrating a model, relatively clean datasets are far more instructive than a large sample

The methodology adopted in this study, where the cuff is placed on the upper arm, is not the only one that can be used. There are potentially several approaches for performing the test. Among various factors affecting FMD, the pressure cuff's position relative to the imaging transducer determines the dilation magnitude and the mediating vasoactive agents (e.g. NO, endothelium-derived hyperpolarizing factor, etc.) [37,39]. However, according to other studies, among them three meta-analyses, the predictive capacity of FMD does not change with the cuff's positioning [39–42]. When the cuff is placed in the proximal position, yielding greater and prolonged dilation [43–45], the discriminative power of FMD is magnified. Further elaboration on the cuff position effect's important consequences for the theory that will be presented will follow in the *Results and Discussion* section.

2.2. Formulation

A surrogate property, $s\left(N/m^2\right)$ (See Fig. 1d), was introduced in our previous studies [1,34], to account for the vasodilators' effect. Since direct access to an individual's vasodilator concentration within their arterial wall after the cuff release is not feasible, the biochemical component of the mechanism underlying the FMD response could not be explicitly incorporated in the model. Therefore, to accommodate the vasodilators' diffusion effect through the arterial wall, the conceptual property, s, was introduced as a theoretical representation of their concentration, and related to their progenitor, namely WSS. Hence, in those studies, s is assumed to take on the instantaneous value of WSS only at the wall's inner radius, from which it starts decreasing as it diffuses outward. As a proxy to the vasodilators' concentration, s is

assumed to obey a first order diffusion law (Eq. (1)).

$$\frac{\partial s}{\partial t} = \alpha_s \left(\frac{\partial^2 s}{\partial r^2} + \frac{1}{r} \frac{\partial s}{\partial r} \right) \tag{1}$$

where $\alpha_s(m^2/s)$, t(s), and r(m) are the diffusivity, time, and the radial distance from the center, respectively. The local value of the wall's elasticity modulus, $E_s(N/m^2)$, that would be reached after a prolonged exposure to a certain value of s, is assumed to asymptotically decrease from a maximum value, E_0 , when s=0, to a minimum value, E_∞ , when $s\to\infty$, following an exponential form as stated by Eq. (2).

$$E_{s}(s) = (E_{0} - E_{\infty})e^{-\beta s} + E_{\infty}$$
 (2)

 β (m^2/N) is a property that is indicative of the wall's resistance to a changing value of s, with a higher value pointing to a lower resistance. As in many biological processes, the modulus' instantaneous value, E(t), is expected to be transient. When the value of s suddenly changes from s_1 to s_2 , E(t) is assumed to transiently change from $E_s(s_1)$ to $E_s(s_2)$ as follows:

$$E(t) - E_s(s_2) = (E_s(s_1) - E_s(s_2))e^{-\xi(t-t_0)}$$
(3)

where ξ (s^{-1}) characterizes the arterial wall's responsiveness to WSS, with a higher value indicating a more responsive artery. Taken together, Eqs. (2) and (3) yield Eq. (4), governing the local instantaneous modulus response to any arbitrary signal s(t).

$$\frac{dE}{dt} + \xi E = \xi E_s(s(t)) \tag{4}$$

The interested reader is referred to our previous papers [1,33] where the steps leading up to Eq. (4) are detailed.

While the arterial wall does exhibit viscoelastic behavior under certain conditions [46], We have already shown that in the context of FMD, the elastic component of the arterial response is overwhelmingly dominant [34]. Therefore, the viscous component of the response will be neglected in this study. The artery's observed slow expansion and eventual recovery makes its mechanical equilibrium quasi-static. Guided by the reported experimental findings [30-32] on the indifference of EC's to purely disturbed and turbulent flows, where only the introduction of a forward WSS component can stimulate the release of vasodilators, only the steady component of the flow rate and the blood pressure will be accounted for. With that said, it must be acknowledged that in 2002, an experimental in vitro study on bovine aortic endothelial cells (BAECs) by Hillsley and Tarbell [47] showed that when a steady shear stress component of 10 dyne/cm2 was augmented by a sinusoidal oscillatory component of 15 dyne/cm2 amplitude at 1 Hz, NO production increased significantly compared to the case of a purely steady shear of 20 dyne/cm². However, we are still opting for exclusively considering the dependence on steady shear for two key reasons. First, the substantial NO production enhancement was only observed after ~1 h of exposure, with the highest enhancement observed after 3 h. On the order of ~5mins though, the timescale within which the FMD test takes place, no significant difference was detected. The other reason is that the added oscillations were sinusoidal, consisting of a single harmonic which can still be considered highly regular. This is far from the case in actual arteries, where the oscillatory shear component consists of many superposed harmonics and therefore resulting in a signal shape that is quite different from that of a simple harmonic [48]. Considering this fact, together with the observations of Noris et al. (1995) on the effect of turbulence (chaotic WSS) on NO production [32], and the flow chamber experimental observations by Chien (2007) on the unresponsive ECs in the disturbed flow reattachment zone [30], it would be more cautious to ignore any oscillatory contributions to vasodilation stimulation in our model, for the time being.

Upon cuff deflation, the abrupt reestablishment of the blood flow rate, $q(m^3/s)$ through the artery when it is still at its narrowest, leads to

a WSS spike, thereby initiating the diffusion of s, which is followed by the arterial dilation, due to softening under the steady component of the blood pressure, $p(N/m^2)$. The blood flow rate during the test was not tracked. This is because in addition to expanding, the artery also moves slightly post cuff deflation, making it especially difficult to keep the lumen within the Doppler sampling gate. Moving the probe to follow the artery will inevitably bring it in and out of focus introducing noise that would undermine our ability to extract the diameter's temporal profile during image processing. The flow rate is therefore assumed to be constant. Evidently, in the real case, it would be expected to at least change slightly. A widely cited 2004 article [43] showed that when the cuff occlusion is proximal, as is the case here, the flow rate exhibits an initial brief, sharp drop and then remains essentially flat around the baseline level for the remainder of the duration post cuff deflation. With that said, if a flow rate signal is reliably acquired in tandem with minimally noisy images of the artery, it can be easily accommodated by

Initially, at its undeformed state, the artery's inner and outer radii are denoted as $r_{in}(m)$ and $r_{out}(m)$, respectively. As the steady component of the WSS, $\tau_w(t)$ corresponds to Poiseuille's parabolic velocity profile, pertinent to the steady component of the flow rate, q, τ_w is then obtained as:

$$\tau_w(t) = \frac{4\mu q}{\pi R(t)^3} \tag{5}$$

where $\mu(kg/m.s)$ and R(t) are the blood's dynamic viscosity and the inner deformed radius, respectively.

The following step of the formulation, in which the dilation stimulation signal at the inner boundary, $s(r_{in}, t)$, will be discussed, is where this study differs from its precursor [1]. Previously, when only the rising-and-dwelling phase was considered, $s(r_{in}, t)$ was assumed to be $\tau_w(t)$ itself, throughout the entirety of that part of the response. However, the peak diameter, at which the artery briefly dwells, is generally greater than its baseline value to which it eventually returns. A greater diameter would imply a lower shear stress at the wall than the baseline value. The fact that the arterial diameter eventually recedes to its baseline suggests that, in the context of this model, the dilation stimulation at the inner boundary starts waning as soon as the baseline is exceeded. This indicates that the wall's cumulative exposure to a shear deficit relative to the shear baseline value, denoted as τ_b , subtracts from $s(r_{in},t)$'s shear component, $\tau_w(t)$, previously assumed [1,34]. Therefore, the mathematical expression of s at the wall's inner boundary in this study is updated as follows:

$$s(r_{in},t) = \tau_w(t) - \zeta \int_0^t H(\tau_b - \tau_w(\theta))(\tau_b - \tau_w(\theta))d\theta$$
 (6)

The integral in Eq. (6) is the cumulative exposure to the shear deficit, $\tau_b-\tau_w$. The Heaviside function, H, is added to ensure that only the deficit is integrated over the shear exposure history. In other words, only when τ_w drops below the baseline value τ_b (when the baseline diameter is exceeded) the deficit exposure starts accumulating. $\zeta(s^{-1})$ is a parameter that quantifies the artery's propensity for recovery. Note how when $\zeta=0$, no subtraction from the shear stimulation takes place, in which case the artery never recovers.

Upon closer inspection, Eq. (6) appears to be alluding to some sort of "memory" for shear deficit, understandably leading the reader to wonder why this does not extend to shear gain exposure as well. If, however, this concept was to be taken to the full extent of its consequences by including the gain exposure going all the way back to the instant after cuff deflation, it would stand to reason to also include the deficit to which the artery is exposed during the 5 min when the flow is choked off. Doing so would make it possible for the value of s to be initially negative which is especially problematic for two reasons: 1. s is intended as a surrogate property to the vasodilators' concentration. A

negative value of s would therefore make no more physical sense than a substance's negative concentration would; 2. Even if we ignore the previous reason and allow for a negative value of s, this will imply that the time it takes the artery's expansion to pick up pace after the cuff is deflated depends on the duration for which the flow was choked off. In principle, this would mean that the artery's expansion onset after cuff deflation can be arbitrarily delayed by prolonging or shortening the initial ischemia. To our knowledge, no such behavior has been observed before.

Before proceeding any further, it's important to elucidate the reasoning behind the way the shifting equilibrium of the dilating arterial wall is modeled. When the smooth muscle cells in the artery's medial layer relax in response to the dilation stimulus, the actin-myosin crossbridging leads to an increase in the reference tissue length, hence contributing to dilation. On the other hand, intra-arterial nitroglycerin (NTG, a vasodilator) treatment led to an increase in arterial tissue compliance [49] while another study showed that it did not affect the brachial artery's stiffness in veterans older than 60 [50]. Blood pressure. among other confounding factors, could also affect the interplay between endothelial function arterial stiffness [51]. Another aspect of the arterial wall that is also involved in its equilibrium is its multilayered structure, with the medial and adventitial layers exhibiting different stiffnesses [52]. Accounting for these effects separately, with no direct noninvasive means of measuring them for each study participant to accommodate natural variability, entails introducing several additional free parameters, which would strain confidence in the uniqueness of their values resulting from the optimization process described later. Instead, these effects are aggregated in an effective single layer wall model, through which a vasodilation signal diffuses and locally changes the tissue compliance (Fig. 1d).

With the problem being axisymmetric, and u(r,t) denoting the radial displacement field, the artery's equilibrium equation is obtained from standard elasticity as:

$$\frac{\partial^2 u}{\partial r^2} + \left(\frac{1}{E}\frac{\partial E}{\partial r} + \frac{1}{r}\right)\frac{\partial u}{\partial r} + \left(\frac{\nu}{Er}\frac{\partial E}{\partial r} - \frac{1}{r^2}\right)u = 0\tag{7}$$

Substituting Eq. (2) in Eq. (4), leads to the equation governing E(r,t):

$$\frac{\partial E}{\partial t} + \xi E = \xi \left[(E_0 - E_\infty) e^{-\beta s} + E_\infty \right] \tag{8}$$

Nondimensionalizing as follows:

$$r^* = \frac{r}{r_{in}}, t^* = \frac{\xi t}{2 \ln(10)}, u^* = \frac{u}{r_{in}}, E^* = \frac{E}{E_0}, s^* = \frac{s}{s_0}$$
 (9)

Eqs. (1), (7) and (8) yield the system governing the FMD process:

$$\frac{\partial^2 u^*}{\partial r^{*2}} + \left(\frac{1}{E^*} \frac{\partial E^*}{\partial r^*} + \frac{1}{r^*}\right) \frac{\partial u^*}{\partial r^*} + \left(\frac{\nu}{E^* r^*} \frac{\partial E^*}{\partial r^*} - \frac{1}{r^{*2}}\right) u^* = 0$$
 (10a)

$$\frac{\partial E^*}{\partial t^*} + 2 \ln(10)E^* = 2 \ln(10) \left[\left(1 - E^*_{min} \right) e^{-Bs^*} + E^*_{min} \right]$$
 (10b)

$$\frac{\partial s^*}{\partial t^*} = 2 \ln(10) \gamma \left(\frac{\partial^2 s^*}{\partial r^{*2}} + \frac{1}{r^*} \frac{\partial s^*}{\partial r^*} \right)$$
 (10c)

The system in Eq. (10) is identical to that of our previous study [1], in which the arising dimensionless parameters are:

$$E_{min}^* = \frac{E_{\infty}}{E_0}, B = \beta s_0, \gamma = \frac{\alpha_s}{r_{io}^2 \xi}, a = \frac{r_{out}}{r_{in}}, p^* = \frac{p}{E_0}$$
(11)

where $s_0 = \frac{4\mu q}{\pi r^3}$.

As elaborated in the earlier study, E_{min}^* is a measure of the wall's sensitivity to WSS. The maximum value of 1 points to an artery that is indifferent to any sensed level of WSS. B describes the artery's resistance to softening due to an increasing WSS. A higher value signifies a lower resistance. The parameter quantifying the mechanotransduction

integrity, γ , indicates how fast the dilation stimulation signal, s, diffuses throughout the arterial wall, as it is directly related to that property's diffusivity, α_s . Eq. (6) gives the inner boundary condition for s(r,t). At the outer boundary where s cannot diffuse any further, its gradient vanishes, $\frac{\partial s}{\partial r}(r_{out},t)=0$. In dimensionless form, the boundary conditions for s^* are:

$$s^{*}(1, t^{*}) = \frac{1}{(1 + \delta(t))^{3}} - 2\ln(10)\zeta^{*} \int_{0}^{t^{*}} H(\delta(z^{*}) - \delta_{b}) \left(\frac{1}{(1 + \delta_{b})^{3}} - \frac{1}{(1 + \delta(z^{*}))^{3}}\right) dz^{*}$$

$$(12a)$$

$$\frac{\partial s^*}{\partial r^*}(a,t) = 0 \tag{12b}$$

where $\zeta^* = \frac{\zeta}{\xi}$, and $\delta = \frac{u(r_{in},t)}{r_{in}}$.

With the outer boundary being load free, and the inner boundary's normal stress being determined from the inner pressure, p, the boundary conditions for u^* are obtained as:

$$\left. \left(\frac{\partial u^*}{\partial r^*} + \nu \frac{u^*}{r^*} \right) \right|_{r^*=1} = \frac{(\nu^2 - 1)p^*}{E^*(1, t)}$$
(13a)

$$\left. \left(\frac{\partial u^*}{\partial r^*} + \nu \frac{u^*}{r^*} \right) \right|_{r^* = a} = 0 \tag{13b}$$

where ν is the Poisson's ratio. With no time yet for any diffusion or softening to take place, the initial conditions at $t^* = 0$ for E^* and s^* are:

$$E^*(r^*,0) = 1$$
 (14a)

$$s^*(r^*,0) = 0 {14b}$$

As Eq. (14a) indicates an initially homogenous wall, the initial gradient of the modulus is zero, $\frac{\partial E}{\partial r}(r,0)=0$, reducing Eq. (10a) to an equidimensional ordinary differential equation that is analytically solved for the initial condition of u^* :

$$u^*(r^*,0) = \frac{p^*}{a^2 - 1} \left[(1 - \nu)r^* + (1 + \nu) \frac{a^2}{r^*} \right]$$
 (15)

Finite difference is implemented to solve the system in Eq. (10) subject to the constraints imposed by Eqs. (13)–(15). The truncation error involved in the discretization of the spatial derivatives is of $O(\delta r^{*3})$ where δr^* is the grid size. The timestep, δt^* , is bounded by a maximum value that is determined from the chosen grid size, to avoid instabilities during the solution of the diffusion equation (Eq. 10c).

$$\delta t_{max}^* = \frac{1}{4\gamma \ln(10) \left(\frac{1}{\delta r^2} - \frac{1}{2\delta r^*(1 + \delta r^*)}\right)}$$
(16)

The same optimization algorithm that we developed and detailed previously [1,33] is used in this study to find the parameter values corresponding to the experimentally observed response by adjusting those values to yield a solution for $\delta(t)$, that results in the least RMS error relative to the experimental response.

To help the reader's intuition in ascribing the model's main parameters to relevant aspects of vascular health, a summary is presented in Table 1. Only the parameters' theoretical ranges are listed as the study involves only 4 subjects, making it impossible to draw any statistically reliable conclusions from the parameter values that were obtained for each subject.

3. Results and discussion

The optimization algorithm used for matching the theory to the experimental measurements is an extension of the one used in our earlier

Table 1A summary of the main model parameters and their meaning.

•		-	
Parameter	Symbol	Relevance to Vascular Health	Theoretical Range
Minimum Stiffness Ratio	E_{min}^*	A higher value indicates more indifference to a changing WSS	$0 \leq E_{min}^* \leq 1$
Softening Parameter	В	A higher value points to an arterial wall that is more receptive to softening	$B \ge 0$
Permeability to Softening Signal	γ	A higher value signifies a more active mechanotransduction	$\gamma \geq 0$
Recovery Parameter	ζ*	A lower value means a weaker tendency to recover	$\zeta^* \geq 0$

work on this subject [33]. Informed by the calculated outer-to-inner diameter ratio, a, the algorithm iterates over the time scale, T = $2\ln(10)/\xi$, $E_{min}^*=rac{E_{\infty}}{E_0}$, $B=eta s_0$, $\gamma=rac{lpha_s}{r_{in}^2\xi}$, $p^*=rac{p}{E_0}$, and $\zeta^*=rac{\zeta}{\xi}$, seeking to minimize the theoretical response's Root Mean Square (RMS) error relative to the measured diameter-vs-time response. In the final, most refined search step, the algorithm sequentially iterates over the free parameters until going a full loop without the RMS error decreasing any further. The resulting theoretical response $\delta(t)$ is then retained as the best fit of the experimental FMD response. Before the paper's conclusion, we dedicate a section to a more elaborate description of the algorithm. Note that ζ^* is the parameter characterizing the recovery phase of the arterial response. Fig. 2 shows a representative matching result. In addition to the curvature shift, a hallmark of mechanotransduction, as it encodes the delay of the arterial tissue's softening in response to the sudden WSS spike in an initially shallow diameter increase that gradually steepens, the recovery phase is also well captured. The agreement between the experimental and theoretical curves is quantified by the Average Instantaneous Error (AIE, where the error relative to the experimental curve is recorded at every instant and the results are averaged for each case). Since these errors are calculated relative to the raw, fluctuating data, they are expected to have a lower bound that is greater than 0 when the fitting curve is devoid of fluctuations.

Fig. 3 shows the matching results for the other cases considered in this study. The experimental data for the case shown in Fig. 3c were acquired in the University of Pennsylvania's Department of Radiology. It is the complete version of a dataset that was used in our prior study [1] where the focus was on the rising-and-dwelling part of the response.

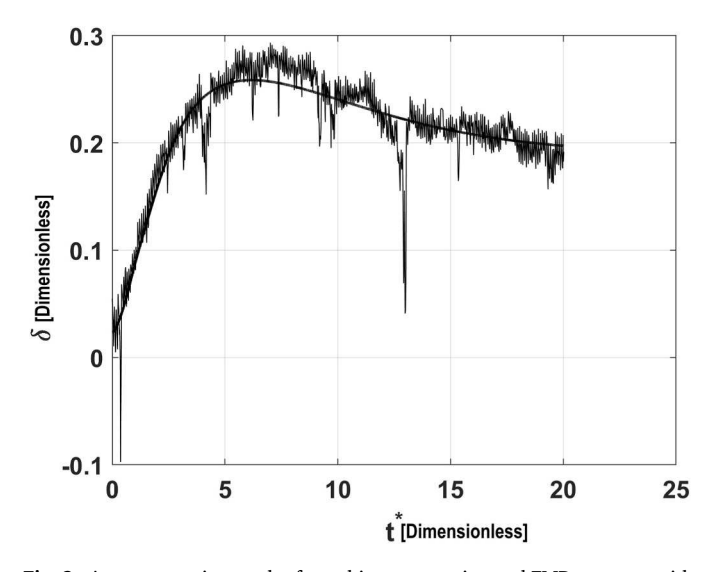


Fig. 2. A representative result of matching an experimental FMD response with its theoretical counterpart (solid thick line). AIE: 10.27 %. x-axis: Dimensionless time. y-axis: Relative deformation (dimensionless).

Demographic information for the case in Fig. 3c is not available as the datasets in that particular study were anonymized such that only the age range of 23-66 was disclosed. As mentioned earlier, given the current study's small sample size and primary objective of showcasing a model that reproduces a typical FMD response, demographic details would not alter the study's main conclusions. The reason behind the lower quality of some of the matches in Fig. 3 (a-c, g) clearly resides in the somewhat noisier experimental data compared to Fig. 2. To find the closest match to an experimental set of data the algorithm looks for the minimum RMS error between the theoretically obtained response and the one that is measured. In doing so, the sudden jumps and falls in the experimental curve, which are inevitably accommodated, lead to instances where the peak of the experimental response is missed by a significant margin as shown in Fig. 3b for example. As clarified in our previous study, these jitters are attributed to artefacts that are due to sudden movements in the subject's arm, leading to faulty frames in the processed ultrasound clip. After enduring a tightly wrapped cuff around their arms for about 5 min and then about another minute and a half until recovery begins, the subjects understandably tend to become a bit restless, which makes inadvertent movements more frequent. This also explains why the noise is predominantly present in the recovery stage of the response. Admittedly, this is a limitation that needs to be addressed in the future. Nevertheless, Figs. 2 and 3 collectively shed light on this novel model's potential when a clean set of experimental data can be obtained.

The above results show that aggregating the molecular and cellular processes underlying FMD into a macroscopically equivalent, single layered wall model, with locally varying compliance, is an effective approach. Our model is predicated on the use of phenomenological parameters that characterize the observed diameter-vs-time response, with each of these parameters having a physical meaning that is intuitively easy to grasp. Any changes in the diameter-vs-time response (which of course would be the manifestation of changes taking place on the microscopic level) can be encoded in variations in the model parameters' values. This theoretical framework provides a more granular, quantitative description of the arterial FMD response (and consequently, vascular health) than that provided by reliance on just FMD%.

Before moving on, further discussion of a significant implication that the cuff position's effect has for the theory is imperative. Rather than being detrimental to the theory's fundamental validity, the FMD response's sensitivity to the cuffing method doubles its diagnostic potential, which was already a substantial improvement from relying on FMD % alone. The reason is as follows.

Among the model's features is the fact that it is not formulated with a specific vasoactive substance in mind. Since the noninvasive nature of the FMD test prohibits real-time access to the biochemical details of the process, s, the conceptual property introduced as a surrogate measure of vasodilators' concentration (Eq. (6)), is the theoretical workaround devised to account for the WSS-mediated vasodilation stimulation. Whether the dominant vasoactive substance is NO, endothelium-derived hyperpolarizing factor, or any other compound is beside the point. One review article [53] reports that FMD resulting from placing the cuff above the probe was reduced from ${\sim}12$ % to ${\sim}7.5$ % when NO was blocked, indicating that the influence of different vasoactive substances is sensitive to the cuff position. This does prove that NO is by no means the sole driver of dilation when this occlusion technique is used. Nevertheless, the numbers above also reveal that NO still contributes about 37.5 % to FMD, which is far from insignificant. As the model can be applied to the artery's diameter vs. time response regardless of where the cuff is placed, the response's sensitivity to the cuff position will be reflected in the resulting model parameter values. In other words, two values, one corresponding to the response resulting from a proximal cuff and the other corresponding to a distal cuff, of each of the model's parameters can now contribute to characterizing vascular health, hence doubling the theory's diagnostic potential.

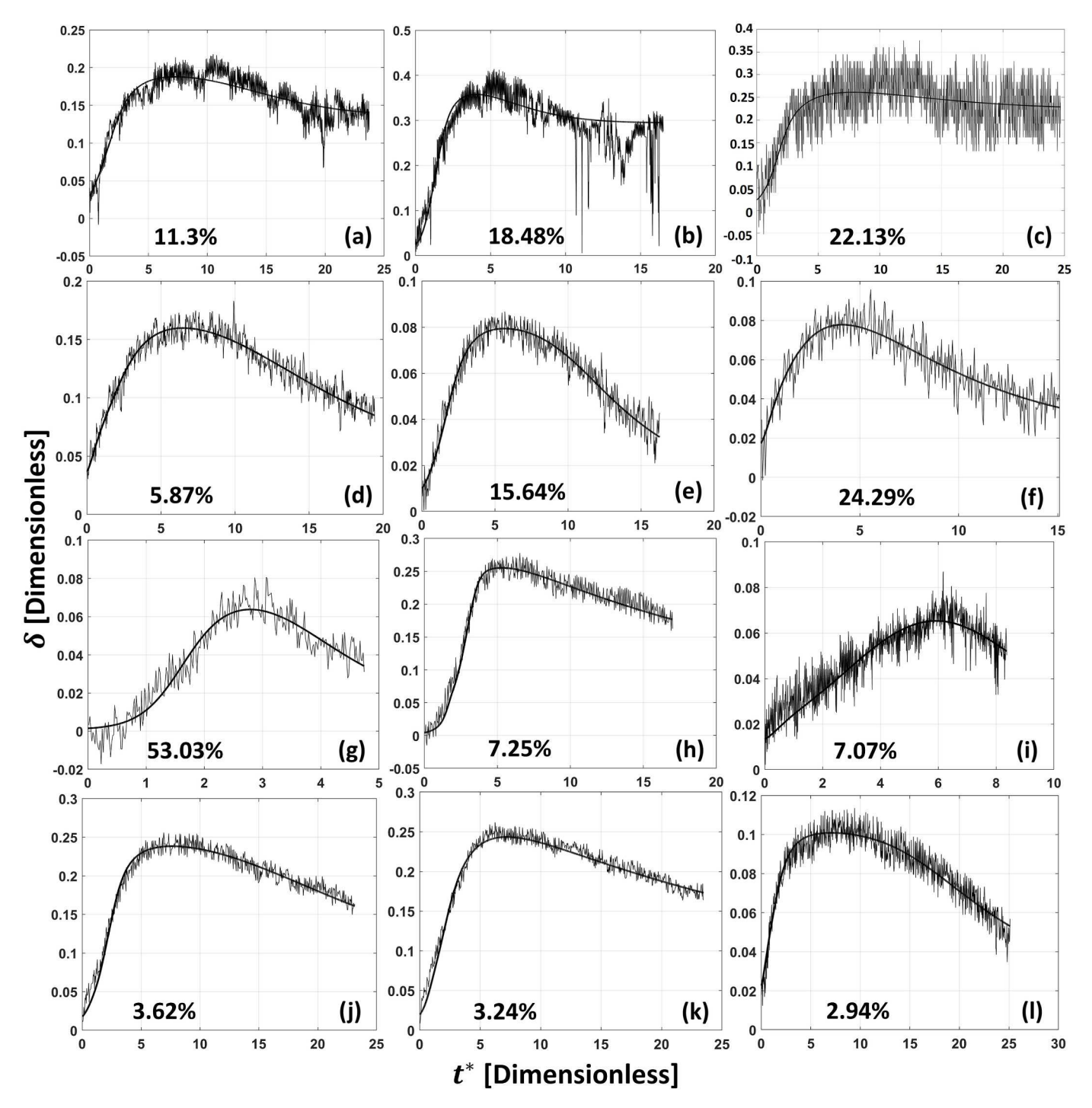


Fig. 3. Matching results for the other considered cases. The listed percentages are the AIE values. x-axis: Dimensionless time. y-axis: Relative deformation (dimensionless).

3.1. Recovery parameter effect

In this section, the recovery parameter's effect (ζ), quantifying the artery's tendency to recover to its baseline diameter, will be discussed. In the previous study [1], the response's sensitivity to E_{min}^* , B, and γ , was illustrated and discussed at length. With E_{min}^* being the minimum stiffness ratio, its value indicates how soft the arterial wall can get. A lower value would allow the artery to eventually get softer, and therefore leading to a higher peak in the response. B, which quantifies the artery's resistance to softening, affects how quickly the artery can soften in response to the pervading dilation stimulation signal, s^* . A lower value

of B indicates a higher resistance, and therefore a higher shear level that is needed by the arterial wall to soften by a given amount. γ , which is the parameter characterizing the strength of mechanotransduction, as it is directly related to the diffusivity α_s (Eq. (11)), describes how fast the stimulation signal, s^* , can reach the outer layers of the arterial wall. A lower value of γ points to a weak mechanotransduction.

The new parameter that was introduced in this study, and which describes the artery's proclivity for recovery after reaching the peak, is ζ^* . From equation (12a), it can be seen that ζ^* is the determinant of the weight that the deficit exposure has in weakening the dilation stimulation at the inner boundary, when the diameter exceeds its baseline. In

the extreme case where $\zeta^*=0$, the shear deficit would be of no significance whatsoever, which would therefore hold the arterial diameter at the reached peak value without ever recovering. Fig. 4 shows the theoretical response for different values of ζ^* . The baseline δ value in this example is set to $\delta_b=0.09$. As ζ^* increases, the onset of recovery moves closer to the peak. Note, however, the slight drop below the baseline when the value of ζ^* is pushed too far ($\zeta^*=0.35$). The stimulation weakening in that case becomes so severe that the slope of the response flattens out after dropping below the baseline. It is for that reason that the change in the value of ζ^* between optimization steps was the most restricted.

3.2. Optimization algorithm

Here, we outline the main elements of the optimization algorithm that we employed to tune the model's parameters to match an observed response. We first estimate p^* and a (Eq. (11)) using the wall's measured inner and outer radii at both baseline $(r_1(\infty))$ and $r_2(\infty)$, respectively) and reactive hyperemia onset $(r_1(0))$ and $r_2(0)$, respectively) where the elasticity modulus, in the context of the presented model, can be assumed uniform. Applying Eq. (15) at both the inner and outer boundaries reveals that:

$$\frac{u^*(a,0)}{u^*(a,\infty)} = \frac{u^*(1,0)}{u^*(1,\infty)} = \frac{E(\infty)}{E(0)}$$
 (17a)

$$\frac{u^*(a,0)}{u^*(1,0)} = \frac{2a}{1 - \nu + (1+\nu)a^2}$$
 (17b)

Using the definitions of u^* (Eq. (9)) and a (Eq. (11)), Eq. (17) can be recast as:

$$\frac{r_2(0) - r_{out}}{r_2(\infty) - r_{out}} = \frac{r_1(0) - r_{in}}{r_1(\infty) - r_{in}}$$
(18a)

$$\frac{r_2(0) - r_{out}}{r_1(0) - r_{in}} = \frac{2r_{in}r_{out}}{(1 - \nu)r_{in}^2 + (1 + \nu)r_{out}^2}$$
(18b)

Defining the terms:

$$A_1 = \frac{r_2(\infty) - r_2(0)}{r_1(\infty) - r_1(0)}, A_2 = \frac{r_2(\infty)r_1(0) - r_2(0)r_1(\infty)}{r_1(\infty) - r_1(0)}$$
 (19a)

$$C_1 = (1 - \nu)r_2(0), C_2 = (1 + \nu)r_2(0)$$
 (19b)

and combining Eqs. (18a) and (18b), it is found that r_{in} is a solution of:

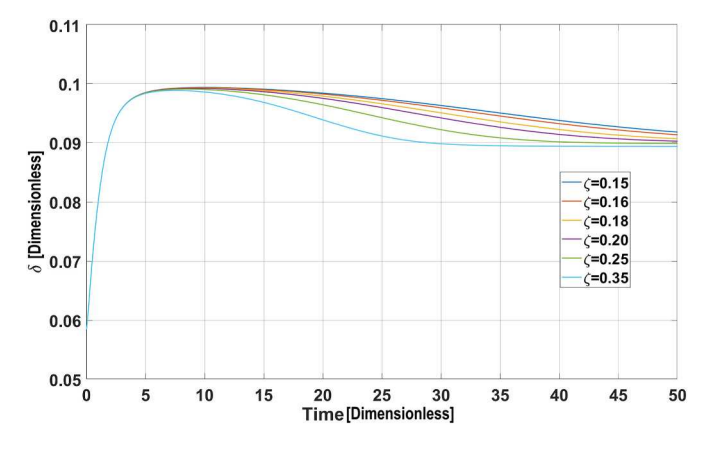


Fig. 4. Effect of ζ^* on the theoretical FMD response. x-axis: Dimensionless time. y-axis: Relative deformation (dimensionless).

$$A_{1}(1+\nu)\left(1-A_{1}^{2}\right)r_{in}^{3}+\left[C_{1}+C_{2}A_{1}^{2}+(1-\nu)A_{2}+3(1+\nu)A_{1}^{2}A_{2}\right.$$
$$\left.-2r_{1}(0)A_{1}-2A_{2}\right]r_{in}^{2}+\left[2A_{2}r_{1}(0)-3(1+\nu)A_{1}A_{2}^{2}\right.$$
$$\left.-2A_{1}A_{2}C_{2}\right]r_{in}+C_{2}A_{2}^{2}+(1+\nu)A_{2}^{3}=0 \tag{20}$$

Arterial tissue is generally assumed to be incompressible, implying a value of ν that is close to 0.5. However, a study [54] on sections of ovine descending aorta reported compressibility yielding values of ν that are as low as about 0.4. A more recent study [55] on porcine arterial walls puts it within 0.3-0.4. In this study, ν is set to 0.4. While clearly desirable, a precise value of ν is not crucial for judging the model's general validity, as may be gathered from the matching results. Indeed, future in-vivo investigations exploring possible effects of hyperemia on ν could guide subsequent refinement of the presented model.

Inspection of the system in Eq. (18) shows that $r_{in}=r_1(0)$, and $r_{out}=r_2(0)$ constitute one of its solutions. This solution should be discarded since those measured values $(r_1(0) \text{ and } r_2(0))$ are the result of the arterial wall being stretched, owing to blood pressure, which means that the sought value of r_{in} is one of the 2 remaining solutions to Eq. (20). It then follows that the other one of the 2 remaining solutions must be real and nonphysical, i.e. negative. Hence, the smaller of Eq. (20)'s two positive solutions should be retained as the value of r_{in} , which is then substituted in Eq. (18a) to obtain r_{out} . The value of a subsequently follows from its definition in Eq. (11). The definition of u^* (Eq. (9)) can then be used to obtain $u^*(1,0)$ which, together with a, yield the value of p^* through Eq. (15). In Fig. 5, a flowchart delineating the next steps of the optimization algorithm is provided.

Note that the step where random deviations are made is added to minimize the chance of getting trapped in a local minimum of the RMS error. It is by no means claimed that this is the only appropriate algorithm. The details of the model's mathematical development are provided earlier to enable researchers who may be interested in the theory to develop a different algorithm, should they deem it necessary for their specific application.

4. Conclusion

4.1. Summary

This paper is the culmination of a series of studies [1,33,34], where the aim is to develop a general theoretical framework describing endothelial mechanotransduction via physics-based modeling of the arterial response during a brachial artery FMD test. While the previous studies focused on the rising-and-dwelling part of the response and managed to reproduce it from more simplified models that were rooted in first principles, this one is extended to include the recovery phase. The conceptual quantity devised as a representation of vasodilation signaling enabled the resulting unified model to successfully reproduce an entire typical FMD response, while being agnostic to the relative magnitudes of different vasoactive agents' effects, depending on the cuffing method. In addition to the parameters previously introduced [1], a new one quantifying the artery's ability to recover arose from the model, hence offering a more detailed description of the arterial physical state. Using ultrasound imaging, experimental FMD data were extracted from healthy volunteers and their corresponding characteristic parameter values were obtained by finetuning the model parameters to match the observed response. A minimally noisy set of data highlights the model's ability to reproduce a real FMD response. It is anticipated that the series of studies [1,33,34] concluded by the current one, will be foundational for the potential emergence of future clinical noninvasive tools that can provide a comprehensive picture describing an individual's arterial health from a simple ultrasound test.

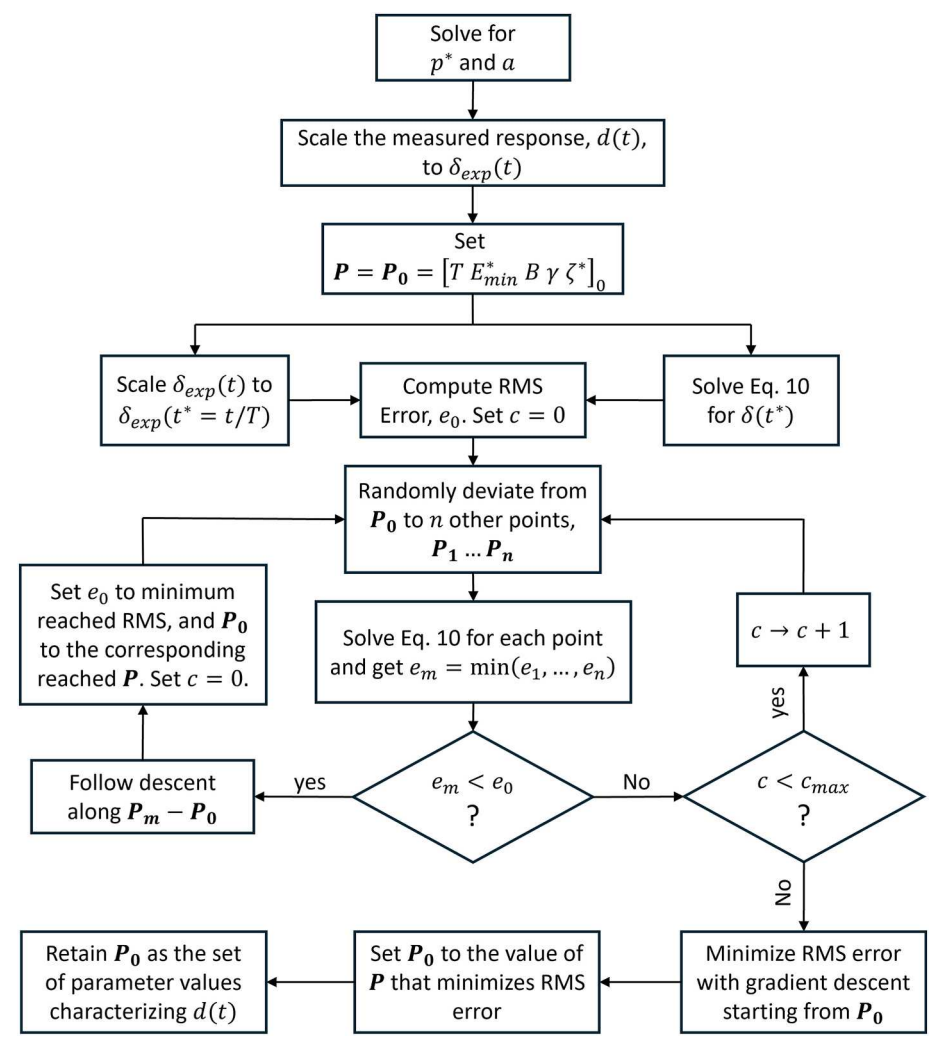


Fig. 5. A flowchart of the optimization algorithm used for matching the theoretical and experimental FMD responses.

4.2. Study limitations and future directions

- Due to the slightly higher noise content in the other datasets, especially during the recovery phase, the quality of the match is reduced.
 This limitation on the experimental side of the study needs to be carefully addressed in the future.
- While the experiments do show that the model works, the small sample size does not permit establishing normal ranges for the model parameters with any degree of confidence. Such an undertaking will require large observational studies where participant groups undergo the FMD test and have their model parameter values extracted and analyzed against the demographic information and biomarker profiles that traditionally inform cardiovascular risk assessment.
- Unlike the case where a known parametrized function is fitted to a given data set, here, a closed form solution to the system in Eq. (10) is not readily available, which makes it much more challenging to ascertain the shape of the cost function (RMS error) being minimized in pursuit of the parameter values characterizing a given FMD response. This is the main reason why the random deviation step is incorporated in the optimization algorithm as a way of mitigating the possibility of being trapped in local minimum, where a simple gradient descent algorithm would remain stuck. Future studies dedicated to charting, or at least approximating the cost function shape potentially enabling the development of more efficient optimization algorithms are warranted.

CRediT authorship contribution statement

Bchara Sidnawi: Writing – review & editing, Writing – original draft, Visualization, Validation, Methodology, Investigation, Formal analysis, Conceptualization. Bingjie Zhou: Writing – review & editing, Visualization, Methodology, Investigation, Data curation. Zhen Chen: Methodology, Data curation. Chandra Sehgal: Writing – review & editing, Supervision, Methodology, Investigation, Funding acquisition, Data curation. Sridhar Santhanam: Writing – review & editing, Supervision, Methodology, Investigation. Qianhong Wu: Writing – review & editing, Supervision, Resources, Project administration, Investigation, Funding acquisition, Data curation, Conceptualization.

Declaration of competing interest

The authors have no conflicts of interest to declare.

Acknowledgment

Q.W., B.S., and B. Z. would like to acknowledge the support of the National Science Foundation under Award No. 2322067 for model development. C.S. and Z.C. would like to acknowledge the support of the National Institute of Health under Award Number R21 EB005326 for experimental data collection.

References

- [1] B. Sidnawi, Z. Chen, C. Sehgal, S. Santhanam, Q. Wu, On the modeling of mechanotransduction in flow-mediated dilation, J. Mech. Behav. Biomed. Mater. 120 (2021) 104606.
- [2] L. Stoner, M. Sabatier, K. Edge, K. McCully, Relationship between blood velocity and conduit artery diameter and the effects of smoking on vascular responsiveness, J. Appl. Physiol. 96 (2004) 2139–2145.
- [3] D.S. Celermajer, et al., Cigarette smoking is associated with dose-related and potentially reversible impairment of endothelium-dependent dilation in healthy young adults, Circulation 88 (1993) 2149–2155.
- [4] T. Nakamura, et al., Endothelial vasomotor dysfunction in the brachial artery predicts the short-term development of early stage renal dysfunction in patients with coronary artery disease. Int. J. Cardiol. 148 (2011) 183–188.
- [5] M. Hashimoto, et al., The impairment of flow-mediated vasodilatation in obese men with visceral fat accumulation, Int. J. Obes. 22 (1998) 477–484.
- [6] K.K. McCully, Flow-mediated dilation and cardiovascular disease, J. Appl. Physiol. 112 (2012) 1957–1958.
- [7] G.K. Birk, et al., Brachial artery adaptation to lower limb exercise training: role of shear stress, J. Appl. Physiol. 112 (2012) 1653–1658.
- [8] K.E. Pyke, M.E. Tschakovsky, The relationship between shear stress and flow-mediated dilatation: implications for the assessment of endothelial function, J. Physiol. 568 (2005) 357–369.
- [9] M. Kaźmierski, A. Michalewska-Włudarczyk, Ł.J. Krzych, M. Tendera, Diagnostic value of flow mediated dilatation measurement for coronary artery lesions in men under 45 years of age, Cardiol. J. 17 (2010) 288–292.
- [10] P. Veluswamy, et al., The sars-cov-2/receptor axis in heart and blood vessels: a crisp update on covid-19 disease with cardiovascular complications, Viruses 13 (2021).
- [11] G. Atkinson, A.M. Batterham, The percentage flow-mediated dilation index: a large-sample investigation of its appropriateness, potential for bias and causal nexus in vascular medicine, Vasc. Med. 18 (2013) 354–365.
- [12] S. Weinbaum, J.M. Tarbell, E.R. Damiano, The structure and function of the endothelial glycocalyx layer. Annu. Rev. Biomed. Eng. 9 (2007) 121–167.
- endothelial glycocalyx layer, Annu. Rev. Biomed. Eng. 9 (2007) 121–167.
 [13] S. Weinbaum, X. Zhang, Y. Han, H. Vink, S.C. Cowin, Mechanotransduction and flow across the endothelial glycocalyx, Proc. Natl. Acad. Sci. U.S.A. 100 (2003) 7988–7995.
- [14] B.M. Fu, J.M. Tarbell, Mechano-sensing and transduction by endothelial surface glycocalyx: composition, structure, and function, Wiley Interdiscip. Rev. Syst. Biol. Med. 5 (2013) 381–390.
- [15] R.H.L. Haeren, et al., Assessment and imaging of the cerebrovascular glycocalyx, Curr. Neurovascular Res. 13 (2016) 249–260.
- [16] J.M. Tarbell, E.E. Ebong, The Endothelial Glycocalyx: A Mechano-Sensor and -Transducer, vol. 1, 2008, pp. 1–6.
- J.M. Tarbell, L.M. Cancel, The glycocalyx and its significance in human medicine,
 J. Intern. Med. 280 (2016) 97–113.
 J.M. Tarbell, M.V. Pahakis, Mechanotransduction and the glycocalyx. J. Intern.
- [18] J.M. Tarbell, M.Y. Pahakis, Mechanotransduction and the glycocalyx, J. Intern. Med. 259 (2006) 339–350.
- [19] Z.D. Shi, G. Abraham, J.M. Tarbell, Shear stress modulation of smooth muscle cell marker genes in 2-D and 3-D depends on mechanotransduction by heparan sulfate proteoglycans and ERK1/2, PLoS One 5 (2010) 1–9.
- [20] Y. Wang, M. Schaffler, S. Weinbaum, A model for the role of integrins in flow induced mechanotransduction in osteocytes, J. Biomech. 39 (2006) S238.
- [21] Y. Zeng, J. Liu, Role of glypican-1 in endothelial NOS activation under various steady shear stress magnitudes, Exp. Cell Res. 348 (2016) 184–189.
- [22] F. Loth, et al., Transitional flow at the venous anastomosis of an arteriovenous graft: potential activation of the ERK1/2 mechanotransduction pathway, J. Biomech. Eng. 125 (2003) 49-61.
- [23] T.W. Secomb, R. Hsu, A.R. Pries, Effect of the endothelial surface layer on transmission of fluid shear stress to endothelial cells, Biorheology 38 (2001) 143–150.
- [24] M.M. Thi, J.M. Tarbell, S. Weinbaum, D.C. Spray, The role of the glycocalyx in reorganization of the actin cytoskeleton under fluid shear stress: a 'bumper-car' model, Proc. Natl. Acad. Sci. U.S.A. 101 (2004) 16483–16488.
- [25] N. Baeyens, et al., Syndecan 4 is required for endothelial alignment in flow and atheroprotective signaling, Proc. Natl. Acad. Sci. U.S.A. 111 (2014) 17308–17313.
- [26] Y. Yao, A. Rabodzey, C.F. Dewey, Glycocalyx modulates the motility and proliferative response of vascular endothelium to fluid shear stress, Am. J. Physiol. Heart Circ. Physiol. 293 (2007) 1023–1030.
- [27] M. Pikoula, M.B. Tessier, R.J. Woods, Y. Ventikos, Oligosaccharide model of the vascular endothelial glycocalyx in physiological flow, Microfluid. Nanofluidics 22 (2018) 1–13
- [28] A.M.W. Bartosch, R. Mathews, J.M. Tarbell, Endothelial glycocalyx-mediated nitric oxide production in response to selective AFM pulling, Biophys. J. 113 (2017) 101–108.
- [29] E.E. Ebong, S.V. Lopez-Quintero, V. Rizzo, D.C. Spray, J.M. Tarbell, Shear-induced endothelial NOS activation and remodeling via heparan sulfate, glypican-1, and syndecan-1, Integr. Biol. 6 (2014) 338–347.

- [30] S. Chien, Mechanotransduction and endothelial cell homeostasis: the wisdom of the cell, Am. J. Physiol. Heart Circ. Physiol. 292 (2007).
- [31] K. Nishida, et al., Molecular cloning and characterization of the constitutive bovine aortic endothelial cell nitric oxide synthase, J. Clin. Invest. 90 (1992) 2092–2096.
- [32] M. Noris, et al., Nitric oxide synthesis by cultured endothelial cells is modulated by flow conditions, Circ. Res. 76 (1995) 536–543.
- [33] B. Sidnawi, Z. Chen, C. Sehgal, Q. Wu, Characterization of arterial flow mediated dilation via a physics-based model, J. Mech. Behav. Biomed. Mater. 107 (2020) 103756.
- [34] B. Sidnawi, S. Santhanam, C. Sehgal, Q. Wu, On the examination of the viscous response of the brachial artery during flow-mediated dilation, J. Mech. Behav. Biomed. Mater. 131 (2022) 105255.
- [35] Y. Yamazaki, Y. Kamiyama, Mathematical model of wall shear stress-dependent vasomotor response based on physiological mechanisms, Comput. Biol. Med. 45 (2014) 126–135.
- [36] Y. Yamazaki, Y. Kondo, Y. Kamiyama, Estimation of shear-stress-induced endothelial nitric oxide production from flow-mediated dilation, Proc. Annu. Int. Conf. IEEE Eng. Med. Biol. Soc. EMBS (2013) 4521–4524, https://doi.org/ 10.1109/EMBC.2013.6610552.
- [37] D.H.J. Thijssen, et al., Expert consensus and evidence-based recommendations for the assessment of flow-mediated dilation in humans, Eur. Heart J. 40 (2019) 2534–2547.
- [38] T. Ma, et al., Flow-mediated dilation analysis coupled with nitric oxide transport to enhance the assessment of endothelial function, J. Appl. Physiol. 131 (2021) 1–14.
- [39] D.J. Green, H. Jones, D. Thijssen, N.T. Cable, G. Atkinson, Flow-mediated dilation and cardiovascular event prediction: does nitric oxide matter? Hypertension 57 (2011) 363–369.
- [40] Y. Matsuzawa, T.G. Kwon, R.J. Lennon, L.O. Lerman, A. Lerman, Prognostic value of flow-mediated vasodilation in brachial artery and fingertip artery for cardiovascular events: a systematic review and meta-analysis, J. Am. Heart Assoc. 4 (2015) 1–15.
- [41] M.C. Corretti, et al., Guidelines for the ultrasound assessment of endothelial-dependent flow-mediated vasodilation of the brachial artery: a report of the international brachial artery reactivity task force, J. Am. Coll. Cardiol. 39 (2002) 257–265.
- [42] E.T.H.C. Smeets, R.P. Mensink, P.J. Joris, Effects of tree nut and groundnut consumption compared with those of L-arginine supplementation on fasting and postprandial flow-mediated vasodilation: meta-analysis of human randomized controlled trials, Clin. Nutr. 40 (2021) 1699–1710.
- [43] A.C. Betik, V.B. Luckham, R.L. Hughson, Flow-mediated dilation in human brachial artery after different circulatory occlusion conditions, Am. J. Physiol. Heart Circ. Physiol. 286 (2004) 442–448.
- [44] S.N. Doshi, et al., Flow-mediated dilatation following wrist and upper arm occlusion in humans: the contribution of nitric oxide, Clin. Sci. 101 (2001) 629–635.
- [45] K.L. Berry, R.A.P. Skyrme-Jones, I.T. Meredith, Occlusion cuff position is an important determinant of the time course and magnitude of human brachial artery flow-mediated dilation, Clin. Sci. 99 (2000) 261–267.
- [46] T. Roy, M.N. Guddati, Full wave simulation of arterial response under acoustic radiation force, Comput. Biol. Med. 149 (2022) 106021.
- [47] M.V. Hillsley, J.M. Tarbell, Oscillatory shear alters endothelial hydraulic conductivity and nitric oxide levels, Biochem. Biophys. Res. Commun. 293 (2002) 1466–1471.
- [48] B. Sidnawi, Z. Chen, C. Sehgal, S. Santhanam, Q. Wu, Characterization of blood velocity in arteries using a combined analytical and Doppler imaging approach, Phys. Rev. Fluids 4 (2019) 1–19.
- [49] A.J. Bank, et al., Direct effects of smooth muscle relaxation and contraction on in vivo human brachial artery elastic properties, Circ. Res. 77 (1995) 1008–1016.
- [50] R.J. Pewowaruk, A.J. Hein, C.M. Carlsson, C.E. Korcarz, A.D. Gepner, Effects of nitroglycerin-induced vasodilation on elastic and muscular artery stiffness in older Veterans, Hypertens. Res. 45 (2022) 1997–2007.
- [51] W. Jin, P. Chowienczyk, J. Alastruey, An in silico simulation of flow-mediated dilation reveals that blood pressure and other factors may influence the response independent of endothelial function, Am. J. Physiol. Heart Circ. Physiol. 318 (2020) H1337–H1345.
- [52] A. Giudici, A.W. Khir, J.M. Szafron, B. Spronck, From uniaxial testing of isolated layers to a tri-layered arterial wall: a novel constitutive modelling framework, Ann. Biomed. Eng. 49 (2021) 2454–2467.
- [53] D.H.J. Thijssen, et al., Assessment of flow-mediated dilation in humans: a methodological and physiological guideline, Am. J. Physiol. Heart Circ. Physiol. 300 (2011) 2–12.
- [54] D.R. Nolan, J.P. McGarry, On the compressibility of arterial tissue, Ann. Biomed. Eng. 44 (2016) 993–1007.
- [55] P. Skacel, J. Bursa, Comparison of constitutive models of arterial layers with distributed collagen fibre orientations, Acta Bioeng. Biomech. 16 (2014) 47–58.